Applied Physics Letters

# 930 kA/cm$^2$ peak tunneling current density in GaN/AlN resonant tunneling diodes grown on MOCVD GaN-on-sapphire template

Cite as: Appl. Phys. Lett. **114**, 203503 (2019); https://doi.org/10.1063/1.5095056
Submitted: 07 March 2019 . Accepted: 09 May 2019 . Published Online: 22 May 2019

Tyler A. Growden, Evan M. Cornuelle, David F. Storm, Weidong Zhang, Elliott R. Brown, Logan M. Whitaker, Jeffrey W. Daulton, Richard Molnar, David J. Meyer, and Paul R. Berger

View Online
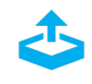
Export Citation

CrossMark

ARTICLES YOU MAY BE INTERESTED IN

Light confinement and high current density in UVB laser diode structure using Al composition-graded p-AlGaN cladding layer
Applied Physics Letters **114**, 191103 (2019); https://doi.org/10.1063/1.5095149

Three-dimensional charge transport mapping by two-photon absorption edge transient-current technique in synthetic single-crystalline diamond
Applied Physics Letters **114**, 203504 (2019); https://doi.org/10.1063/1.5090850

Bandgap narrowing and Mott transition in Si-doped $Al_{0.7}Ga_{0.3}N$
Applied Physics Letters **114**, 113501 (2019); https://doi.org/10.1063/1.5086052

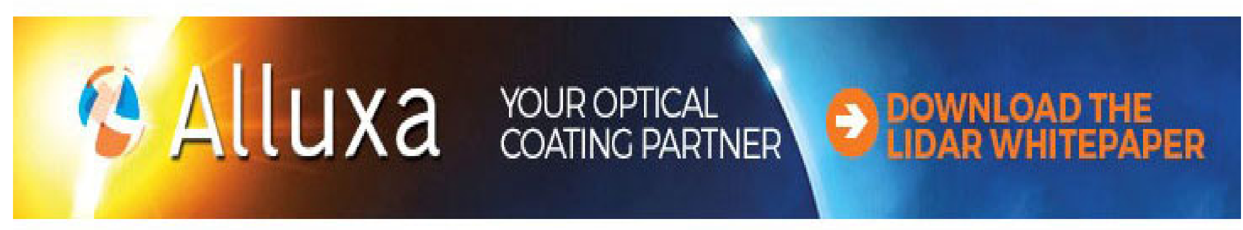

# 930 kA/cm$^2$ peak tunneling current density in GaN/AlN resonant tunneling diodes grown on MOCVD GaN-on-sapphire template

Cite as: Appl. Phys. Lett. **114**, 203503 (2019); doi: 10.1063/1.5095056
Submitted: 7 March 2019 · Accepted: 9 May 2019 ·
Published Online: 22 May 2019

Tyler A. Growden,[1,a] Evan M. Cornuelle,[2] David F. Storm,[1] Weidong Zhang,[3] Elliott R. Brown,[3] Logan M. Whitaker,[2] Jeffrey W. Daulton,[4] Richard Molnar,[4] David J. Meyer,[1] and Paul R. Berger[2]

## AFFILIATIONS

[1]U.S. Naval Research Laboratory, Washington, DC 20375, USA
[2]Department of Electrical and Computer Engineering, The Ohio State University, Columbus, Ohio 43210, USA
[3]Departments of Physics and Electrical Engineering, Wright State University, Dayton, Ohio 45435, USA
[4]Lincoln Laboratory, Massachusetts Institute of Technology, Lexington, Massachusetts 02421, USA

[a]Author to whom correspondence should be addressed: tyler.growden.ctr@nrl.navy.mil

## ABSTRACT

We report on the design and fabrication of ultrahigh current density GaN/AlN double barrier resonant tunneling diodes grown via rf-plasma assisted molecular-beam epitaxy. The device structure was grown on a metal-organic chemical vapor deposition GaN-on-sapphire template. The devices displayed repeatable room temperature negative differential resistance with peak tunneling current densities ($J_p$) between 637 and 930 kA/cm$^2$. Analysis of temperature dependent measurements revealed the presence of severe self-heating effects, which allow strong phonon scattering that deteriorates the electron quantum transport. Finally, a qualitative comparison to the same structure grown on a low dislocation density freestanding GaN substrate has shown that sapphire-based templates are a feasible alternative.

https://doi.org/10.1063/1.5095056

Resonant tunneling diodes (RTDs) in III-nitride material systems have been of interest in recent years. The wide bandgap and high carrier mobility of III-nitrides have potential to increase power output and operating temperature of RTDs. Early work in III-nitride RTDs grown on GaN-templated sapphire substrates suffered from charge-trapping, hysteresis, nonrepeatability, high dislocation densities, and lack of room temperature negative differential resistance (NDR).[1–14] Clear and repeatable resonant tunneling based NDR in III-nitride RTDs was first observed in growths on high quality free-standing bulk GaN substrates.[15–19] Production of large-area free-standing bulk GaN substrates remains a challenge so that highly uniform, thick GaN templates atop sapphire substrates are an attractive alternative because of their low relative manufacturing cost and ease of producing large wafer sizes. This in turn facilitates process integration and high-volume manufacturing. Very recently, repeatable and reproducible resonant tunneling based NDR in GaN/AlN heterostructures grown on sapphire substrates was reported;[20] however, the current density remained low ($\sim$6 kA/cm$^2$). It is worth mentioning, however, that they did observe a second NDR region at $\sim$11 V which displayed a current density of 164 kA/cm$^2$.

In this letter, we investigate the feasibility of transferring an evolving high current density GaN/AlN RTD technology from bulk GaN substrates to sapphire substrates with GaN templates. The NDR from early GaN-based RTDs grown on GaN templates was not repeatable across multiple voltage sweeps and therefore has been argued to be a result of charge-trapping effects, rather than conventional resonant tunneling.[14] As with most thin vertical devices, one of the main sources of concern is the substrate dislocation density. There exists a 14% lattice mismatch between a GaN template and sapphire substrate which results in a highly dislocated interfacial region. Consequently, even with a thick GaN buffer, dislocation densities are generally $>10^8$ cm$^{-2}$ for GaN-on sapphire substrates. In GaN, dislocations can act as nonradiative recombination centers,[21] charged scattering centers, or leakage current pathways,[22] all of which are highly detrimental to a vertical device. Another possible consequence of the lattice mismatch may be an increase in roughness at the heterointerfaces in the active region. Both dislocations and interface roughness can scatter electrons, degrading quantum transport. Nevertheless, here we show that some of these issues can be addressed with advanced growth techniques which facilitate repeatable NDR in ultrahigh current density GaN/AlN RTDs.

The RTD structure [illustrated in Fig. 1(a)] was grown by rf-plasma assisted molecular-beam epitaxy (rf-MBE) atop a GaN template that was itself grown by metal-organic chemical vapor deposition (MOCVD) on (0001) sapphire. The GaN template consisted of a 2 $\mu$m-thick Fe-doped layer followed by a 2 $\mu$m-thick undoped layer. The Fe-doped layer introduces acceptorlike point defects which allow for the subsequent growth of semi-insulating material by compensating for residual impurities in GaN which would otherwise render it n-type. The density of extended defects was estimated to be $\sim 3 \times 10^8\,\text{cm}^{-2}$ on the basis of defect-counting over a given area of an atomic force microscopy (AFM) image.

To prepare for MBE growth, the templated GaN wafer was first degreased in organic solvents and etched in a 5:25:7 $NH_4OH$:$H_2O$:$H_2O_2$ ("SC1") solution immediately prior to loading in the ultrahigh vacuum (UHV) system and then degassed under UHV conditions for 30 min at 600 °C. The device layers were grown in a Scienta Omicron Pro-75 MBE chamber equipped with a Veeco Uni-Bulb® nitrogen plasma source. Ga and Al were supplied by a standard dual filament effusion cell and a Veeco Sumo® effusion cell, respectively. Silicon doping was accomplished using a single-filament medium-high temperature effusion cell. The nitrogen plasma source was operated at a constant power and nitrogen flow of 275 W and 0.80 sccm, respectively, resulting in a growth rate of ~3 nm/min. The gallium-to-active nitrogen ($Ga/N^*$) flux ratio was approximately 1.7, while the $Al/N^*$ flux ratio was estimated to be just slightly greater than unity. All layers were grown continuously without interruption at a constant temperature of 860 °C as indicated by a thermocouple mounted behind the substrate. Upon completion of the growth, the as-grown surface was observed to be free from gallium droplets, indicating that the excess gallium desorbed from the surface during growth. Greater details on the growth procedure can be found elsewhere.[23]

The sample was processed using five photolithography mask steps and standard device processing methods. The first photo-mask defined the top contact, and electron beam (e-beam) evaporation was used to deposit a Ti/Al/Ti/Au/Ni (20/100/30/50/20 nm) metal stack. The mesa was then dry-etched with a $Cl_2$/$BCl_3$/Ar inductively coupled plasma reactive ion etch (ICP-RIE) process, using the sacrificial top Ni layer as the mask. Following the mesa definition, a second photo-mask was used to define the bottom contact, which was identical to the top contact. Device isolation pads were defined using a third photo-mask followed by the same ICP-RIE recipe used for the mesa. The protective Ni layer for the top contact was then removed using HCl, and a 500 nm layer of silicon nitride was deposited by plasma enhanced chemical vapor deposition (PECVD) for sidewall passivation and device encapsulation. Vias were then created using a fourth photo-mask and dry-etched by a $CF_4$-based ICP-RIE process. Finally, a Ti/Au (20/400 nm) ground-signal-ground (GSG) pad was defined with the fifth photo-mask.

Figure 1(b) displays the typical current-voltage (I-V) characteristics for two representative devices of different sizes (6 and 11 $\mu m^2$). During I-V measurements, the voltage was swept from −4 V to +5.5 V and back down to −4 V. The smallest area devices (6 $\mu m^2$) were the only ones to display room temperature NDR [Fig. 1(b)]. In all of the devices which displayed NDR, there was a chairlike structure observed in the NDR region [illustrated in Fig. 1(c) inset]. This structure is commonly observed in RTDs and thought to be a result of either intrinsic bistability[24] (energy level of quasibound states in the quantum well being dependent upon tunneling current) or extrinsic bistability[25–27] (rectification of a self-oscillation). Due to the polarization-induced field present in III-nitride RTDs, they have an asymmetric structure in which the charge buildup at resonance is enhanced, which would imply that an intrinsic bistability is possible; however, it is still being investigated. Between devices of the same size, the peak voltage, $V_p$, remained quite stable [illustrated in Fig. 1(c)]. However, the peak current varied moderately over ~20 mA, resulting in a range of peak tunneling current densities from 637 to 930 kA/cm$^2$, as shown in Fig. 1(c). The exact source of this variation is unknown, but it is being explored further. While this is the largest current density reported for a III-nitride RTD, we would only expect to have around 10% of the current available for oscillator applications, as the power output is estimated to be $\frac{3}{16}\Delta I \Delta V$ (Ref. 28), where $\Delta I$ is the difference between the peak and valley current and $\Delta V$ is the difference between the valley and the peak voltage. However, despite the small peak-to-valley current ratios (PVCRs), the available current densities, $\Delta J$, approach 100 kA/cm$^2$. A $\Delta J$ this high can result in very low RC time delays and large power output, thus creating the potential for high-speed, high-power RTD-based GaN devices.

As the mesa area increased from 6 to 11 $\mu m^2$, the NDR region disappeared and was replaced by an inflection in the I-V, which occurred at higher voltages. This increase in voltage is likely due to increased contact resistance resulting from greater $I^2R$ Joule heating through a contact pad which is, nominally, the same size. In high current density RTDs, the effects of self-heating have also been shown to cause a significant increase in the valley current[17,29] because of the larger junction temperature. This increases phonon scattering, especially from longitudinal optical (LO) phonons and piezoelectric acoustic phonons. If the self-heating is strong enough, the valley current will overtake the peak current, thus masking the NDR. Because these effects scale with area, it is likely the cause of the NDR being masked in the I-V curve of the 11 $\mu m^2$ device displayed in Fig. 1(b). It should also be noted that, while generally thought of as contributing very little, LO-phonon assisted resonant tunneling (LO-phonon emission) has been shown to contribute to the valley current in RTDs.[30,31]

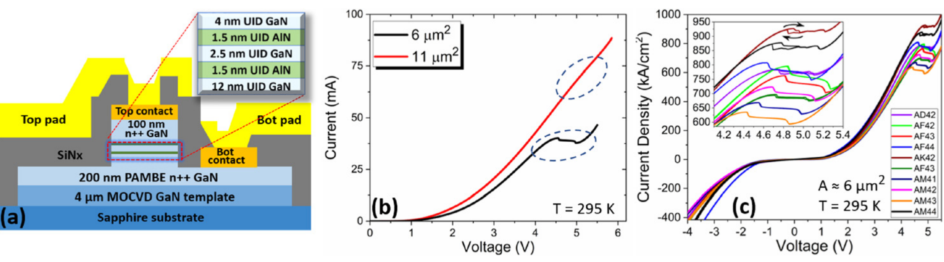


FIG. 1. (a) Fabricated device layout and (inset) as-designed active region. (b) Room temperature current-voltage characteristics of two different sized devices. (c) Current density vs voltage from ten different operational devices of the same dimensions illustrating the difference in peak current density.

To better understand the origin of the inflated valley current, temperature dependent I-V measurements were carried out at twelve different temperatures ranging from 8 K up to 297 K on 6 $\mu$m$^2$ and 11 $\mu$m$^2$ devices with a Lakeshore CRX-6.5K cryogenic probe station [displayed in Figs. 2(a) and 2(b)]. For the 6 $\mu$m$^2$ device (AM44) in Fig. 2(a), it was observed that the PVCR increases from 1.02 at 295 K up to 1.40 at 8 K as a result of valley current suppression. The peak current was very stable with temperature, which indicates very little contribution from thermionic emission; however, $V_p$ did shift from +4.85 to +5.07 V as it was cooled, but this is to be expected. More notably, the 11 $\mu$m$^2$ device (AF24) in Fig. 2(b), which only displayed an inflection at room temperature, began displaying NDR ~225 K, which continued to improve until 8 K, at which point it reached a maximum PVCR of 1.32. The drop of valley current suggests the suppression of phonon scattering processes as the temperature decreases in the presence of significant self-heating effects. This behavior is expected, to some degree, at current densities this large. However, it is possible that the lower thermal conductivity of the sapphire wafer (33.9 W/m K, Ref. 32), compared to GaN (254 W/m K, Ref. 33), could exacerbate these effects. Because the peak current does not change with temperature, but the valley current does, we can develop an approximation, based on a theoretical model by Ridley *et al.*[34] and the assumption that incoherent phonon-assisted valley tunneling current is proportional to the inverse of the scattering time, to estimate the current contributions from various mechanisms

$$I_v \approx C_0 + C_1 T + C_2 e^{\frac{-\hbar\omega_{LO}}{k_B T}}, \tag{1}$$

where the first term (with $C_0$ a constant) represents a combination of current from interface roughness scattering, dislocation scattering (edge and mixed), and direct shorts from screw dislocations; the second term (with $C_1$ a constant) represents current from acoustic phonon scattering; and the third term (with $C_2$ a constant) represents current from optical phonon scattering. A value of 92 meV was used for the LO-phonon energy in GaN. It should be mentioned that this estimation treats the first term as a "catch-all" for any source of temperature independent scattering or leakage mechanisms, but it is likely dominated by the dislocations. Figure 2(c) displays Eq. (1) fitted to $J_v(T)$ for both devices (AM44 and AF24). The adjusted R-squared value for both was ≈0.99, indicating a very good fit. Using the values obtained from this fit, the estimated contributions to the valley current density for each term vs temperature are plotted in Fig. 2(d). The current density associated with the dislocations and interface roughness scattering appear to dominate in both devices. The difference observed in this first term is likely caused by a variation in dislocation density, barrier thickness, or possibly sidewall leakage. The contribution from both acoustic and optical phonons appears to be similar; however, the larger device, AF24, does increase faster. This likely has to do with increased self-heating from $I^2R$ resistive losses, resulting in a greater junction temperature. It is important to note that Eq. (1) and Figs. 2(c) and 2(d) are meant to give a qualitative view of the various mechanisms which contribute to the unusually large valley current densities which have been observed in GaN-based RTDs.

To gain greater insight into the effects of using an MOCVD GaN template on sapphire, we compared the results being reported here to those of our previously reported high current GaN/AlN RTDs on free-standing GaN substrates.[17] The sapphire-based template has a dislocation density of $\sim 3\times10^8$ cm$^{-2}$ compared to $\leq 1\times10^7$ cm$^{-2}$ of bulk

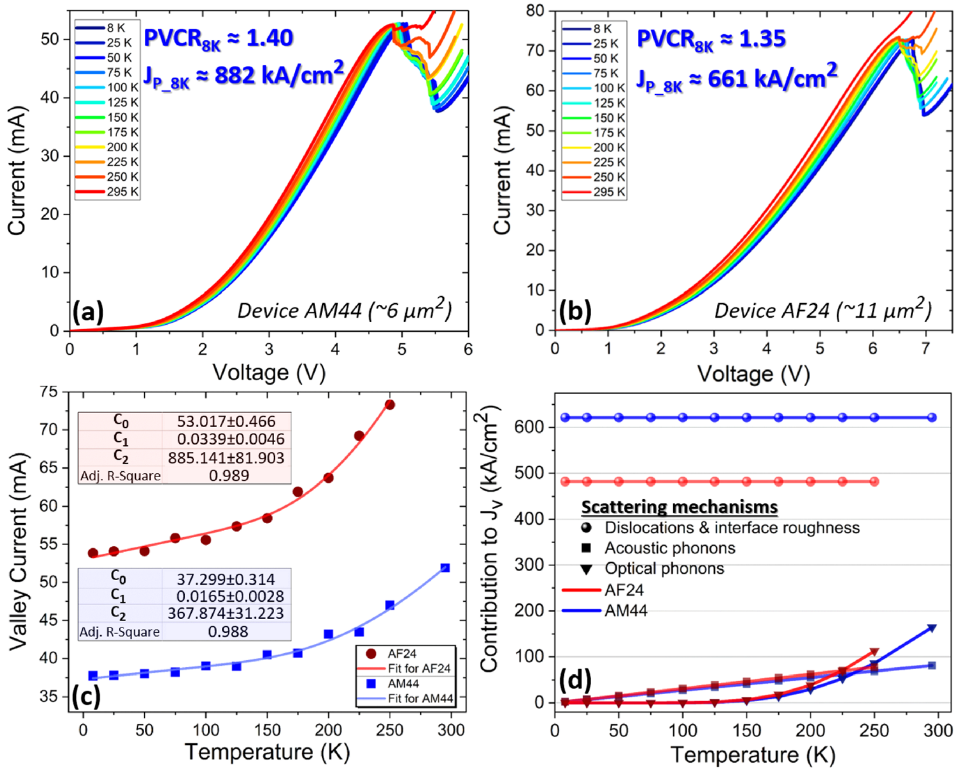


FIG. 2. Low temperature I-V characteristics for (a) 6 $\mu$m$^2$ (AM44) and (b) 11 $\mu$m$^2$ (AF24) devices. (c) An exponential fit of the valley current vs temperature for AM44 and AF24. (d) Estimation of valley current density contributions from dislocation and interface roughness scattering, acoustic phonon scattering, and optical phonon scattering for both devices.

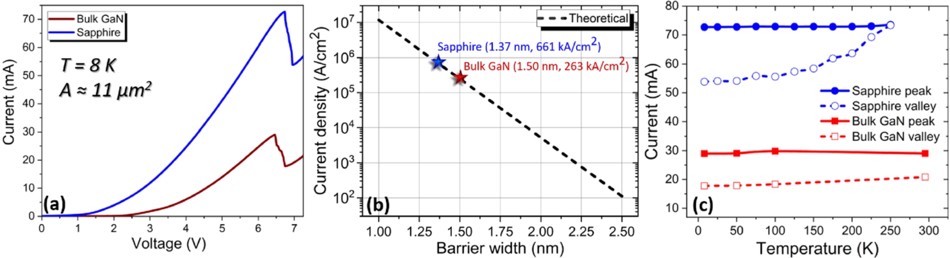


**FIG. 3.** Comparison of (a) dc I-V characteristics for identical RTD structures grown on a bulk GaN substrate vs a MOCVD GaN template on sapphire [reported previously Ref. 17 and also displayed in Fig. 1(a) in this report]. (b) A plot, generated by utilizing a quantum transport solver, displaying the relationship between peak current and AlN barrier width. (c) The peak and valley current values for both samples vs temperature.

GaN. The design [displayed in Fig. 1(a)] and growth of the two samples were the same. The only differences for the sapphire sample were a modified pregrowth clean and during processing, SiNx was used in lieu of $SiO_2$ as the passivation/isolation layer on exposed surfaces. It should also be mentioned that the growths were done nearly two years apart, but in the same MBE chamber. That being said, this comparison is meant to be more qualitative than quantitative.

Displayed in Fig. 3(a) are the I-V characteristics for equal area (11 $\mu$m$^2$) devices from both samples at 8 K. The comparison of I-V characteristics in Fig. 3(a) suggests a very similar form with nearly identical peak voltages. Inflection points are present below the main peak at voltages around +2.0 and +3.0 V for the sapphire and bulk GaN devices, respectively. These inflections are a telltale sign of resonant tunneling through lower quantum-well energy levels than associated with the main peak and with much lower values of current density so that NDR does not occur. However, the peak tunneling current differs by ~250%. We speculate that the effective growth temperature of the RTD structure on sapphire was 40–50 °C higher than for the nominally identical growth on freestanding GaN due to the significantly lower thermal conductivity of sapphire (33.9 W/m K, Ref. 32) compared to GaN (254 W/m K, Ref. 33). We further speculate that this difference in real growth temperature resulted in AlN barrier layers which were up to 10% thinner in the RTD structure on sapphire compared to the structure on freestanding GaN. This possibility is currently being investigated. The properties of RTDs are such that even a single monolayer deviation in the active region can significantly impact the device performance. Previous research has shown both experimentally and theoretically that the current of an RTD scales exponentially with barrier thickness.[29,35] Using a nonequilibrium Green's function (NEGF) quantum transport solver,[36] the structure was simulated over the same range of bias voltage, and the peak current was extracted for multiple barrier thicknesses and plotted in Fig. 3(b). This simulation was previously developed and fitted to the data obtained from the bulk GaN samples.[17] Superimposed on this curve are the peaks for both samples based on their current density. For a current density of 661 kA/cm$^2$ (sapphire), a barrier thickness of ~1.37 nm is predicted, approximately 10% less than the nominal thickness of 1.5 nm. Additionally, another possible contribution to the increased current is likely due to increased leakage resulting from a larger dislocation density in the sapphire sample. It has been reported that only pure screw dislocations in GaN are conductive and that they comprise roughly 10% of the total dislocation density.[22] Therefore, we can expect a screw dislocation density in the GaN template of $\sim 3 \times 10^7$ cm$^{-2}$. We can estimate the probability of finding $n$ dislocations, $P(n)$, for a given area A and areal density $\rho$, using the Poisson probability density function as follows:

$$P(n) = \frac{(\rho A)^n}{n!} e^{-\rho A}. \quad (2)$$

The probability of an 11 $\mu$m$^2$ sapphire device having no screw dislocations is thus ~3.7%, whereas for the bulk GaN, it is ~89%. This makes three assumptions that are reasonable in the two samples: (1) that the percentage of screw dislocations in a bulk GaN crystal is similar to that of a MOCVD GaN template on sapphire, (2) that no new dislocations were generated during the MBE growth for either sample, and (3) the occurrence of any given dislocation is uncorrelated with the others.

The peak current and valley current are plotted vs temperature in Fig. 3(c) for both the sapphire and bulk GaN samples. The behavior of the peak current is very stable for both samples. However, the valley current increases more rapidly in the sapphire sample. This is likely associated with greater heat generation resulting from a larger current; however, it could also be a consequence of lower thermal conductivity.

In summary, we have reported experimental data for GaN/AlN RTDs grown on sapphire substrates. The device design was identical to that of our previously reported high current density RTDs on freestanding GaN substrates, thus allowing for a direct comparison. By moving to a sapphire-based GaN template, the dislocation density increased by more than an order of magnitude. Despite the high dislocation density, room temperature NDR with peak tunneling current densities as high as 930 kA/cm$^2$ was achieved. However, room temperature NDR was only observable on the smallest devices. Temperature dependent measurements ranging from 8 K up to 300 K revealed NDR on the larger area devices below a certain threshold temperature. Using the data from the temperature dependent measurements, an estimation was made which qualitatively described the valley current contributions from different scattering and leakage pathways. The comparison between sapphire-based templates and freestanding GaN substrates has shown that substrate choice does affect the valley current. However, this study has also shown that even with a dislocation density of $\sim 10^8$ cm$^{-2}$, vertical devices, such as the RTD, can still be realized. Further analysis of the leakage mechanisms associated with substrate choice for GaN-based RTDs will likely lead to greater valley current suppression and, subsequently, much improved PVCRs.

This work was supported by the U.S. National Science Foundation (under Collaborative Grant Nos. ECCS-1711731 and

ECCS-1711733), Program Director Dr. Dimitris Pavlidis, and the Office of Naval Research. The authors would like to thank Brian Downey for helpful discussions. DISTRIBUTION STATEMENT A. Approved for public release. Distribution is unlimited. This material is based upon work supported by the Under Secretary of Defense for Research and Engineering under Air Force Contract No. FA8702-15-D-0001. Any opinions, findings, conclusions or recommendations expressed in this material are those of the author(s) and do not necessarily reflect the views of the Under Secretary of Defense for Research and Engineering.

## REFERENCES

[1]A. Kikuchi, R. Bannai, K. Kishino, C. M. Lee, and J. I. Chyi, Appl. Phys. Lett. **81**, 1729 (2002).
[2]K. Kishino and A. Kikuchi, Phys. Status Solidi A **190**, 23 (2002).
[3]S. N. Grinyaev and A. N. Razzhuvalov, Semiconductors **37**, 433 (2003).
[4]C. T. Foxon, S. V. Novikov, A. E. Belyaev, L. X. Zhao, O. Makarovsky, D. J. Walker, L. Eaves, R. I. Dykeman, S. V. Danylyuk, S. A. Vitusevich, M. J. Kappers, J. S. Barnard, and C. J. Humphreys, Phys. Status Solidi C **0**, 2389 (2003).
[5]M. Hermann, E. Monroy, A. Helman, B. Baur, M. Albrecht, B. Daudin, O. Ambacher, M. Stutzmann, and M. Eickhoff, Phys. Status Solidi C **1**, 2210 (2004).
[6]S. Golka, C. Pflugl, W. Schrenk, and G. Strasser, Appl. Phys. Lett. **88**, 172106 (2006).
[7]C. Bayram, Z. Vashaei, and M. Razeghi, Appl. Phys. Lett. **96**, 042103 (2010).
[8]Z. Vashaei, C. Bayram, and M. Razeghi, J. Appl. Phys. **107**, 083505 (2010).
[9]L. Yang, H. He, W. Mao, and Y. Hao, Appl. Phys. Lett. **99**, 153501 (2011).
[10]T. A. Growden, S. Krishnamoorthy, D. N. Nath, A. Ramesh, S. Rajan, and P. R. Berger, in *70th Annual Device Research Conference, The Pennsylvania State University, University Park, PA, 18–20 June 2012* (IEEE, 2012), pp. 163–164.
[11]D. Li, L. Tang, C. Edmunds, J. Shao, G. Gardner, M. J. Manfra, and O. Malis, Appl. Phys. Lett. **100**, 252105 (2012).
[12]D. Li, J. Shao, L. Tang, C. Edmunds, G. Gardner, M. J. Manfra, and O. Malis, Semicond. Sci. Technol. **28**, 074024 (2013).
[13]A. Grier, A. Valavanis, C. Edmunds, J. Shao, J. D. Cooper, G. Gardner, M. J. Manfra, O. Malis, D. Indjin, Z. Ikonic, and P. Harrison, J. Appl. Phys. **118**, 224308 (2015).
[14]A. E. Belyaev, C. T. Foxon, S. V. Novikov, O. Makarovsky, L. Eaves, M. J. Kappers, and C. J. Humphreys, Appl. Phys. Lett. **83**, 3626 (2003).
[15]T. A. Growden, D. F. Storm, W. Zhang, E. R. Brown, D. J. Meyer, P. Fakhimi, and P. R. Berger, Appl. Phys. Lett. **109**, 083504 (2016).
[16]J. Encomendero, F. A. Faria, S. M. Islam, V. Protasenko, S. Rouvimov, B. Sensale-Rodriguez, P. Fay, D. Jena, and H. G. Xing, Phys. Rev. X **7**, 041017 (2017).
[17]T. A. Growden, W. Zhang, E. R. Brown, D. F. Storm, K. Hansen, P. Fakhimi, D. J. Meyer, and P. R. Berger, Appl. Phys. Lett. **112**, 033508 (2018).
[18]J. Encomendero, R. Yan, A. Verma, S. M. Islam, V. Protasenko, S. Rouvimov, P. Fay, D. Jena, and H. G. Xing, Appl. Phys. Lett. **112**, 103101 (2018).
[19]T. A. Growden, W. Zhang, E. R. Brown, D. F. Storm, D. J. Meyer, and P. R. Berger, Light: Sci. Appl. **7**, 17150 (2018).
[20]D. Wang, J. Su, Z. Chen, T. Wang, L. Yang, B. Sheng, S. Lin, X. Rong, P. Wang, X. Shi, W. Tan, J. Zhang, W. Ge, B. Shen, Y. Liu, and X. Wang, Adv. Electron. Mater. **5**(2), 1800651 (2019).
[21]S. J. Rosner, E. C. Carr, M. J. Ludowise, G. Girolami, and H. I. Erikson, Appl. Phys. Lett. **70**, 420 (1997).
[22]J. W. P. Hsu, M. J. Manfra, D. V. Lang, S. Richter, S. N. G. Chu, A. M. Sergent, R. N. Kleiman, L. N. Pfeiffer, and R. J. Molnar, Appl. Phys. Lett. **78**, 1685 (2001).
[23]D. F. Storm, T. A. Growden, W. Zhang, E. R. Brown, N. Nepal, D. S. Katzer, M. T. Hardy, P. R. Berger, and D. J. Meyer, J. Vac. Sci. Technol., B **35**(2), 02B110 (2017).
[24]V. J. Goldman, D. C. Tsui, and J. E. Cunningham, Phys. Rev. Lett. **58**, 1256 (1987).
[25]H. C. Liu, Appl. Phys. Lett. **53**, 485 (1988).
[26]T. C. L. G. Sollner, E. R. Brown, and W. D. Goodhue, in *Picosecond Electronics and Optoelectronics II*, edited by F. J. Leonberger, C. H. Lee, F. Capasso, and H. Morkoc (Springer, Berlin, 1987), p. 103.
[27]T. J. Foster, M. L. Leadbeater, L. Eaves, M. Henini, O. H. Hughes, C. A. Payling, F. W. Sheard, P. E. Simmonds, and G. A. Toombs, Phys. Rev. B **39**(9), 6205 (1989).
[28]C. S. Kim and A. Brändli, IRE Trans. Circuit Theory **8**, 416 (1961).
[29]T. P. E. Broekaert and C. G. Fonstad, J. Appl. Phys. **68**, 4310 (1990).
[30]V. J. Goldman, D. C. Tsui, and J. E. Cunningham, Phys. Rev. B **36**, 7635 (1987).
[31]H. Mizuta and T. Tanoue, in *The Physics and Applications of Resonant Tunnelling Diodes*, edited by H. Ahmed, M. Pepper, and A. Broers (Cambridge University Press, Cambridge, 1995).
[32]A. Hofmeister, Phys. Chem. Miner. **41**, 361 (2014).
[33]H. Shibata, Y. Waseda, H. Ohta, K. Kiyomi, K. Shimoyama, K. Fujito, H. Nagaoka, Y. Kagamitani, R. Simura, and T. Fukuda, Mater. Trans. **48**, 2782 (2007).
[34]B. K. Ridley, B. E. Foutz, and L. F. Eastman, Phys. Rev. B **61**, 16862 (2000).
[35]D. H. Chow, J. N. Schulman, E. Ozbay, and D. M. Bloom, Appl. Phys. Lett. **61**, 1685 (1992).
[36]See www.silvaco.com for "Silvaco ATLAS (software), 2016."